Radiocarbon, Vol 60, Nr 1, 2018, p 113–135 DOI:10.1017/RDC.2017.91

RADIOCARBON AND STABLE ISOTOPE EVIDENCE FOR CHANGES IN SEDIMENT MIXING IN THE NORTH PACIFIC OVER THE PAST 30 KYR

Kassandra M Costa[1,2*] • Jerry F McManus[1,2] • Robert F Anderson[1,2]

[1]Lamont-Doherty Earth Observatory of Columbia University, Palisades, NY 10964, USA.
[2]Department of Earth and Environmental Sciences, Columbia University, New York, NY 10027, USA.

ABSTRACT. Deep-sea sediment mixing by bioturbation is ubiquitous on the seafloor, and it can be an important influence on the fidelity of paleoceanographic records. Bioturbation can be difficult to quantify, especially in the past, but diffusive models based on radioactive tracer profiles have provided a relatively successful approach. However, a singular, constant mixing regime is unlikely to prevail in a region where dynamic oceanographic changes in the bottom water environment are a consequence of paleoclimatic variability. In this study, foraminiferal stable isotopes, radiocarbon (^{14}C) dating, and ^{230}Th fluxes are utilized to understand the sediment mixing history in the easternmost region of the North Pacific. In the uppermost sediment, a 12,000-yr offset between planktonic foraminifera species *N. incompta* and *G. bulloides* is observed that coincides with age plateaus at 2000–2500 yr for *N. incompta* and 15,000–16,000 yr for *G. bulloides* despite coincident glacial-interglacial shifts in δ^{18}O of benthic species. These age plateaus, particularly for *G. bulloides*, are a result of changing foraminiferal abundance related to assemblage shifts and carbonate preservation changes since the last glacial period, providing a window into the extent of mixing in the past. The ^{14}C and stable isotope results can be simulated using an iterative model that couples these changes in foraminiferal abundance with variability in mixing depth over time. The best-fit model output suggests that the deepest, or most intense, mixing of the past 30,000 yr (30 kyr) may have occurred during the Holocene. Even though changes in mixing affect the ^{14}C and δ^{18}O of planktonic species that have dramatically varying abundance, substantial age control is nevertheless provided by δ^{18}O measurements on the more consistently abundant benthic foraminifera *Uvigerina*, thus allowing the construction of a reliable chronology for these cores.

KEYWORDS: bioturbation, North Pacific, radiocarbon, stable isotopes.

INTRODUCTION

A central tenet of sediment stratigraphy is the progressive aging of sediment with increasing depth. In a static setting, sediment settles in neat, successive layers. Yet the marine sediment–water interface is a dynamic environment in which gravitational slumping, bottom water remobilization, and bioturbation intervene with stratigraphic sediment deposition. Bioturbation is particularly confounding; its ubiquity operates as a low pass filter on sediment records (Berger and Heath 1968; Guinasso and Schink 1975; Goreau 1980; Wheatcroft et al. 1990; Boudreau 1994; Anderson 2001; Laepple and Huybers 2014), but it can sometimes occur in discrete channels that create a heterogeneous age distribution in the sediment and possibly even age reversals (Ruddiman and Glover 1972; Berger and Johnson 1978; Anderson 2001). Constraining the influence of bioturbation and other sediment mixing processes is particularly important in interpreting high-frequency climate proxy records, particularly with regards to their amplitude and duration (Bard et al. 1987; Anderson 2001; Trauth 2013; Laepple and Huybers 2014).

Sediment mixing is often parameterized using radioactive tracers like ^{210}Pb and ^{14}C (Peng et al. 1979; Demaster and Cochran 1982), which have known input functions and decay rates such that the distribution of these tracers within the sediment renders an estimate of sediment mixing in the ocean. The short half-life of ^{210}Pb ($t_{1/2} = 22.3$ yr) limits its utility to only the modern mixing depth, but long-lived ^{14}C ($t_{1/2} = 5730$ yr) can trace sediment mixing well into the last glacial period (Peng et al. 1979). Because sediment mixing can vary with environmental parameters, the assumption of a constant mixing regime over time may be an oversimplification of sedimentary conditions. Variations in the availability of organic carbon, as a food source, and dissolved oxygen, to support respiration, are each likely influences on benthic mixing. For example, low oxygen concentrations in bottom waters can suffocate benthic communities such

*Corresponding author. Email: kcosta@ldeo.columbia.edu.

that sediment accumulates in undisturbed, laminated deposits (Behl and Kennett 1996; Yarincik et al. 2000; Cook et al. 2005; Davies et al. 2011). If oxygen concentrations change over time, then it would not be unreasonable to expect the intensity of sediment mixing to change as well. In the Pacific Ocean, previously observed variability in sediment remobilization (Kienast et al. 2007) and oxygen concentrations (Cook et al. 2005; Jaccard and Galbraith 2012; Jaccard et al. 2014; Praetorius et al. 2015; Tetard et al. 2017) during the rapid climate transitions of the deglaciation suggest that the intensity of sediment mixing may have indeed fluctuated during this period. Linking sediment mixing to environmental conditions may have the potential to allow predictions of the nature and timing of changes to bioturbation and its influence on sedimentary records. This study presents new radiocarbon (^{14}C) and oxygen isotope records to mutually constrain a model of sediment mixing in the Northeast Pacific Ocean over the past 30,000 yr (30 kyr).

STUDY SITE AND METHODOLOGY

The Juan de Fuca Ridge (JdFR) is located in the Northeast Pacific Ocean about 500 km off the coast of North America in the subpolar transition zone (Figure 1). Sediment cores were collected from the JdFR on the SeaVOICE cruise (AT26-19) of the R/V Atlantis in September 2014. Sedimentation rates on the ridge are highly variable (from <0.5 to >3 cm/kyr) as a result of both glacial-interglacial carbonate preservation cycles and sediment focusing and winnowing along the rough bathymetry of the ridge (Costa et al. 2016; Costa and McManus 2017). Glacial sediments are characterized by high carbonate content, high dry bulk density, low magnetic susceptibility (terrigenous content), and higher coarse fraction (primarily foraminiferal tests) (Costa et al. 2016). Previous work has focused on piston cores, which provide long records (up to 700,000 yr ago, or 700 ka) but poor recovery of more recent sediment. To study the last glacial maximum, deglaciation, and Holocene, this study utilizes samples from four multicores (AT26-19-53MC, -13MC, -10MC, and -06MC) and one trigger core (AT26-19-23TC) that were

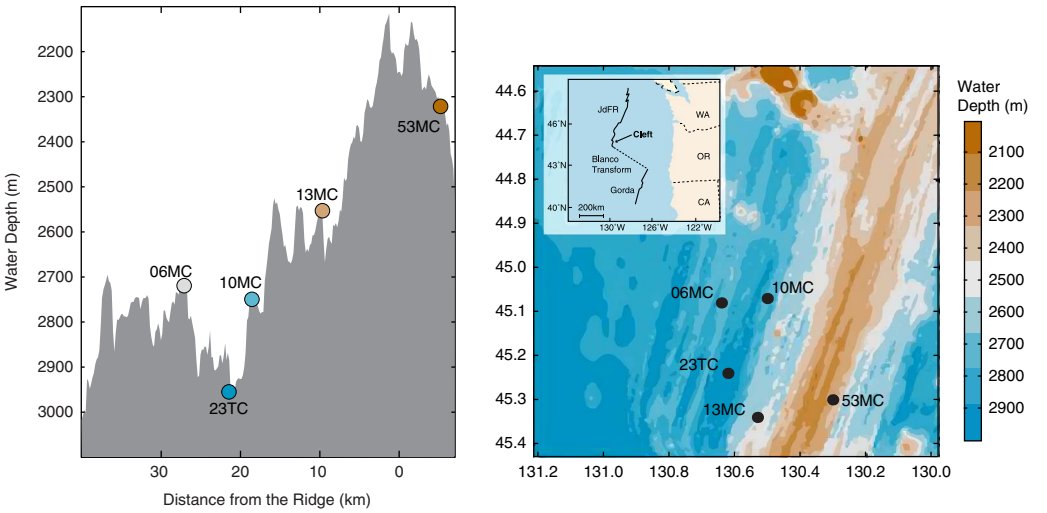

Figure 1 Core locations on the Juan de Fuca Ridge. (Right) Bathymetric map showing the location of the cores relative to the ridge crest (in orange), modified from Costa et al. (2016). (Left) Representative bathymetric profile from the ridge crest to the ridge flanks. Core locations are superimposed on this profile, although their exact depth and distance location may differ slightly. Cores generally follow a depth transect: 53MC, 2347 m; 13MC, 2503 m; 06MC, 2668 m; 10MC, 2711 m; and 23TC, 2906 m. (Color refers to online version.)

https://doi.org/10.1017/RDC.2017.91 Published online by Cambridge University Press

retrieved in a depth gradient from the ridge crest (53MC, 2347 m) to the most proximal abyssal valley (23TC, 2906 m) (Figure 1). Two of the multicores (06MC and 10MC) correspond with previously published piston cores (09PC and 12PC, respectively) (Costa et al. 2016).

Stable Isotope Analyses

Gentle deployment of multi-corers allows the recovery of the sediment–water interface, but the presence of water within the sediment barrels can potentially disturb the upper sediment layers during transport and storage. To minimize these effects, multicores were slabbed shipboard into 1-cm slices immediately upon recovery. Samples from 23TC, a gravity core, were taken later at the Lamont-Doherty Earth Observatory (LDEO) core repository. All samples were then freeze-dried, and an aliquot was weighed into a 125 mL Nalgene bottle: average ~4 g for 23TC and average ~20 g for multicores, the large sample size permitted by the full barrel slabs taken shipboard. The bottles were filled with approximately 100 mL of tap water, and disaggregated on a tumble wheel for 2 hr. Samples were then sieved at 63 μm, and a soft brush was used to gently break up clay clumps that did not sufficiently disintegrate during tumbling.

Oxygen isotopes in foraminifera largely record ice volume, temperature, and salinity, but they can also vary systematically by size fraction, in response to physiological effects, like the presence or absence of symbionts, as well as their depth habitat, seasonality, and stage in the reproductive cycle (Erez 1978; Bemis et al. 1998; Spero 1998; Ezard et al. 2015). To determine the most representative size fraction, stable isotopes were analyzed from *Uvigerina* sp., *Cibicidoides* sp., *Globigerina bulloides*, *Neoglobigerina pachyderma*, and *Neoglobigerina incompta* (formerly *Neoglobigerina pachyderma dextral*) in different size fractions on a Thermo Delta V Plus equipped with a Kiel IV individual acid bath device at LDEO. Although no size fractionation of oxygen isotopes was observed in *N. pachyderma*, *G. bulloides*, or *Cibicidoides* sp., *Uvigerina* sp. demonstrates a positive size relationship, in which $\delta^{18}O$ increases with increasing size fraction, and *N. incompta* exhibits the opposite size relationship (see supplementary Figure 1). These results inform the size fraction that would be the best compromise between the diverse size fraction trends and the economies of picking foraminifera from larger (e.g., more massive) sizes. All subsequent $\delta^{18}O$ data presented here were picked from the 250–300 μm fraction, approximately the midpoint of the *Uvigerina* sp. and *N. incompta* size trends, and a size range in which generally fewer than 10 tests are sufficiently massive for isotopic analysis. Analyses of benthic species generally utilized 2–3 individuals, while analyses of planktonic species were based on 8–12 individuals. Although a greater number of individuals (preferably 30+) would provide greater confidence in capturing a normal distribution of values that would better represent the population, analyzing such large numbers of foraminifera was precluded by relatively low foraminiferal abundance. More than 50% of the samples had less than 10% coarse fraction, reflecting the generally poor carbonate preservation of the region.

Foraminiferal assemblage counts were conducted on core 13MC at select sediment intervals. An average of 560 individuals were counted from unbiased sediment splits of the 250–300 μm fraction for *Uvigerina* sp., *Cibicidoides* sp., *G. bulloides, N. pachyderma, N. incompta*, *G. ruber,* other unspecified planktic foraminifera, and other unspecified benthic foraminifera to recreate the population of foraminifera present in the sediment. These census counts allow the calculation of relative abundances (e.g., % *G. bulloides* of all planktic species), concentrations (e.g., # *G. bulloides* specimens/g sediment), and burial fluxes (e.g., # *G. bulloides* specimens/cm^2 kyr).

https://doi.org/10.1017/RDC.2017.91 Published online by Cambridge University Press

Radiocarbon Analyses

Radiocarbon dates ($n = 29$) from the five sediment cores were analyzed, using 300–500 tests of either *G. bulloides* or *N. incompta*. While *G. bulloides* was present in samples from all depths, the relative abundance of *N. incompta* increased towards the coretop. In cores 06MC and 10MC, only *N. incompta* had sufficient mass in the shallowest sample for the ^{14}C analyses, while only *G. bulloides* had sufficient mass for the deeper samples. In core 13MC, each sample depth except the deepest provided sufficient mass to analyze both *G. bulloides* and *N. incompta* for ^{14}C. All samples for 53MC are from *G. bulloides*. Analyses were performed at the National Ocean Sciences Accelerator Mass Spectrometry Facility at Woods Hole Oceanographic Institution. ^{14}C ages were calibrated to calendar years using Calib 7.0 Marine13 (Stuiver and Reimer 1993; Reimer et al. 2013) with a total reservoir correction of 800 yr ($\Delta R = 400$).

Total Particle Flux Analyses

Total particle flux calculations were determined using ^{230}Th normalization, as detailed by Costa and McManus (2017). Briefly, samples were analyzed for thorium (^{230}Th, ^{232}Th) and uranium (^{238}U, ^{235}U, ^{234}U) by isotope dilution inductively coupled plasma mass spectrometry following complete acid digestion and column chromatography (Fleisher and Anderson 2003). Unsupported ^{230}Th was isolated by correcting for lithogenic and authigenic uranium decay (Henderson and Anderson 2003), and the initial deposition concentration was calculated by correcting for ^{230}Th decay (half-life of 75,584 yr; Cheng et al. 2013). The short residence time of ^{230}Th (20–40 yr; Nozaki et al. 1981) translates into nearly all of the ^{230}Th produced by uranium decay in seawater being removed locally to sediments by scavenging. Therefore, the concentration of excess ^{230}Th in the underlying sediment is primarily a function of the particle flux, such that higher particle flux will dilute the excess ^{230}Th concentration in the sediment. The particle flux can be calculated as the integrated ^{230}Th production in the overlying water column divided by the concentration of excess ^{230}Th in the sediment corrected for decay since deposition (Bacon 1984; McManus et al. 1998; Henderson and Anderson 2003; Francois et al. 2004). Comparing the burial inventory of ^{230}Th with the inferred production of ^{230}Th in the overlying water column reflects the degree of sediment focusing (Ψ) during the period of sediment deposition (Suman and Bacon 1989).

RESULTS

Oxygen Isotopes and Foraminiferal Assemblage

Oxygen isotope records (*Uvigerina* sp., *Cibicidoides* sp., *G. bulloides*, *N. pachyderma*, *N. incompta*) are presented for each core in Figure 2. Reproducibility based on complete replicate samples averages 0.23‰ for all species. The benthic $\delta^{18}O$ records (*Uvigerina* sp., *Cibicidoides* sp.) largely correspond to the global trend that reflects changes in ice volume and temperature associated with the last deglaciation (Lisiecki and Stern 2016). The deepest samples reach glacial values (4.5–5‰, *Uvigerina* sp.) while shallower coretop values (3.5–4‰, *Uvigerina* sp.) are more consistent with an interglacial (Holocene) period. No water depth dependent isotope effect is apparent, and the absolute values as well as the temporal trends in *Uvigerina* sp. $\delta^{18}O$ are equivalent across all five cores. Oxygen isotopes from *Cibicidoides* sp. are generally well correlated with those of *Uvigerina* sp. ($r^2 = 0.73$) with an average offset of –0.52‰, slightly less than the widely applied offset of –0.64‰ (Shackleton 1973) but consistent with a relatively low offset (–0.4 to –0.5‰) previously observed in North Pacific sediments (Keigwin 1998). Furthermore, recent re-evaluation of *Cibicidoides* and *Uvigerina* $\delta^{18}O$ suggests that the global offset may be closer to -0.47 ± 0.04‰ (Marchitto et al. 2014).

https://doi.org/10.1017/RDC.2017.91 Published online by Cambridge University Press

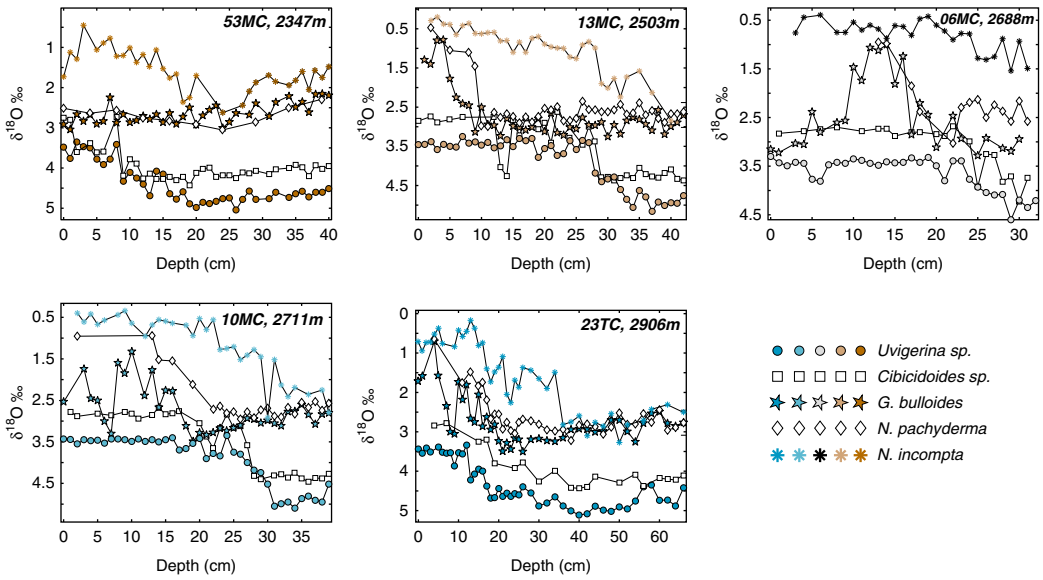

Figure 2 Oxygen isotope records for *Uvigerina* sp., *Cibicidoides* sp., *G. bulloides, N. pachyderma,* and *N. incompta* for each of the five cores. Symbols are as shown in the legend, but color-coded for each individual core. Errors (not shown for clarity) are based on replicated analyses (n values): 0.21‰ for *Uvigerina* sp. ($n=98$), 0.16‰ for *Cibicidoides* sp. ($n=50$), 0.25‰ for *G. bulloides* ($n=57$), 0.30‰ for *N. pachyderma* ($n=29$), and 0.25‰ *N. incompta* ($n=67$). (Color refers to online version.)

The robust glacial-interglacial transition in the *Uvigerina* sp. data facilitates the stratigraphic alignment of the five cores independent of any age assignment. The *Uvigerina* sp. $\delta^{18}O$ were graphically correlated onto a single "composite" depth scale (Figure 3), and the depth alignment was then applied to the other isotope records. Comparisons of core depths with composite depths are provided in supplementary Figure 2. Core 13MC was used as a reference due to its clear glacial-Holocene transition and its relatively stable sedimentation rate. The composite depths of 53MC are shifted ~15 cm deeper than the core depths, but other adjustments to align 53MC with 13MC amount to small (≤1%) deviations in the original age/depth relationship. The first 20 cm of 06MC are identical (±3%) in core depth and composite depth, while deeper samples are compressed onto the composite deglacial depth trend. Aligning 10MC depth to the composite depths requires only minor adjustments on the order of ±7%, primarily in the older part of the core. The higher sedimentation rate in 23TC requires a more substantial change in the depth domain to align it with the composite depths. The first 12 cm of 23TC are shifted downwards by 7 cm and then stretched by a factor of 2/3. The rest of the core is then compressed by a factor of 2/3 in order to align the *Uvigerina* sp. $\delta^{18}O$ with those on the composite depth scale. The fidelity of these alignments is corroborated by the small range in *Uvigerina* sp. $\delta^{18}O$ variability at any one composite depth interval (Figure 3). A glacial-interglacial transition is also defined by the composite *Cibicidoides* sp. $\delta^{18}O$ record, but a few glacial type values appear up to 10 cm composite depth for this species. The coherency of the $\delta^{18}O$ of these benthic species amongst the five cores is likely a function of the relatively low but stable benthic foraminiferal flux over the time interval investigated in this study.

Planktonic $\delta^{18}O$ records (*G. bulloides*, *N. pachyderma*, *N. incompta*) show considerable interspecies variability. Of the three species, only *N. incompta* demonstrates a clear glacial to Holocene transition (Figure 3), and thus its temporal trend mimics those of the benthic species

https://doi.org/10.1017/RDC.2017.91 Published online by Cambridge University Press

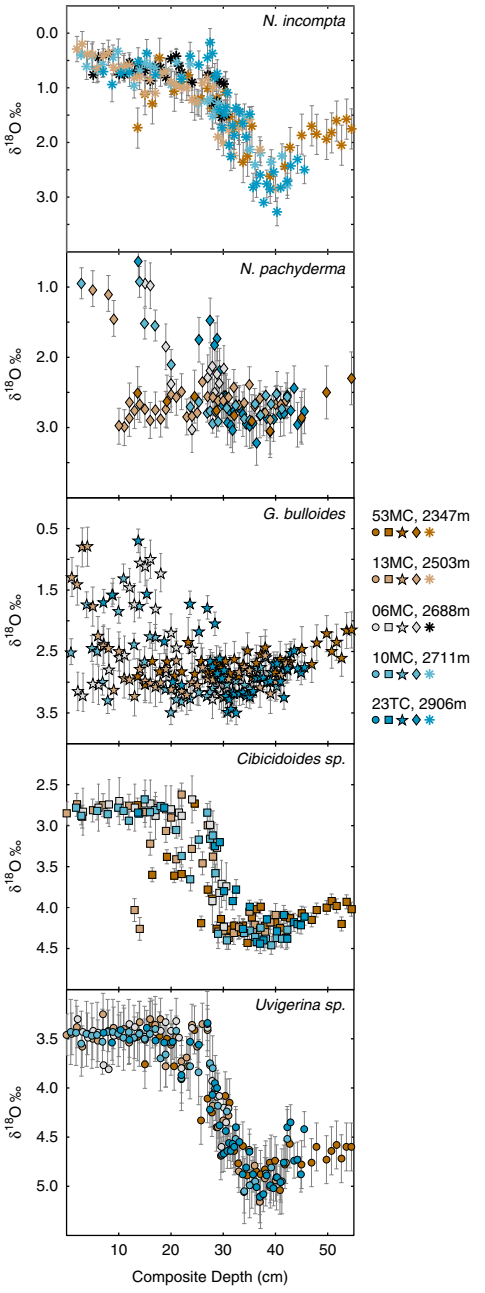

Figure 3 Oxygen isotope records on a composite depth scale, aligned based on the $\delta^{18}O$ of *Uvigerina* sp. The small inter-core variability in $\delta^{18}O$ of *Uvigerina* sp. as well as *N. incompta* indicates the stratigraphic integrity on a regional scale. Composite $\delta^{18}O$ records of *Cibicidoides* sp., *G. bulloides*, and *N. pachyderma* demonstrate increasing degrees of variability between the five cores. Error bars reflect the 2σ of replicate analyses.

https://doi.org/10.1017/RDC.2017.91 Published online by Cambridge University Press

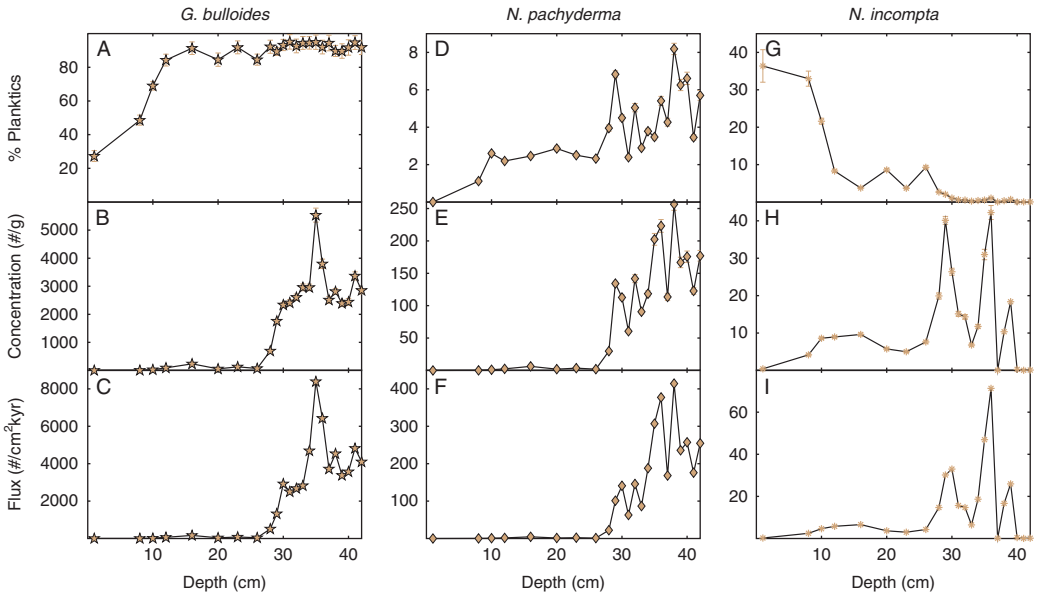

Figure 4 Foraminiferal assemblage of core 13MC. Top panels (A, D, G) show the relative composition of the total planktic population. For most of the sedimentary record, *G. bulloides* is the dominant (>85%) planktic species (A). In coretop samples, *N. incompta* becomes an important species in the sediment assemblage as well (G). Error bars reflect 1σ uncertainty derived from counting statistics of the total number of specimens identified. Middle panels (B, E, H) show the total concentration of each species per gram of sediment (dry weight). Note the different scales on the *y*-axis for each species. Bottom panels (C, F, I) show the ^{230}Th-normalized total flux of each species. Again, note the different scales on the *y*-axis for each species.

($r^2 = 0.70$ with *Uvigerina* sp.; $r^2 = 0.59$ with *Cibicidoides* sp.). Deep samples have higher $\delta^{18}O$ (2.5–3‰) while shallower coretop samples have lower $\delta^{18}O$ (0–1‰). In 13MC (2503 m) the *N. incompta* proportion of the sediment assemblage increases at shallower depths, from less than 1% up to 36% of all planktic species (Figure 4G). There are several peaks in concentration and flux at 29 cm, 36 cm, and 39 cm, but the variability is small, just one order of magnitude (Figure 4H and 4I).

Oxygen isotopes from neither *G. bulloides* nor *N. pachyderma* adhere to the expected deglacial changes in ice volume and temperature, as demonstrated by the benthic species and *N. incompta,* although poor recovery of *N. pachyderma* in shallower sediments may contribute to this appearance (Figure 3). *N. pachyderma* is a relatively minor component of the sediment assemblage, ranging from 0 to only 8.2% of the burial population (Figure 4D). *G. bulloides*, on the other hand, is the dominant species throughout most of the sedimentary record: it makes up greater than 85% of the planktic species up until 12 cm, after which its relative abundance decreases as *N. incompta* abundance rises (Figure 4A). Despite comprising a small percentage of the population, *N. pachyderma* achieves concentrations and fluxes that span over two orders of magnitude, reaching values as high as 257 specimens/g and 414 specimens/ cm^2 kyr at 38 cm, and reflecting a general decline in flux towards shallower depths (Figures 4E and 4F). *G. bulloides* shows the greatest variability, so that even while it is comprising the majority of the planktic assemblage, its concentration and flux range over three orders of magnitude (Figures 4B and 4C). It shows a similar declining flux towards shallower depths as *N. pachyderma*, and there is a single clear abundance peak in *G. bulloides* at 35 cm with a concentration of 5530 specimens/g and a flux of 8390 specimens/cm^2 kyr.

https://doi.org/10.1017/RDC.2017.91 Published online by Cambridge University Press

There is also a strong isotopic trend with water depth for *G. bulloides* and *N. pachyderma*. The shallowest core, 53MC (2347 m), shows almost no change in $\delta^{18}O$ in these species over the entire core: *N. pachyderma* ranges from 2.3 to 3.0‰ while *G. bulloides* ranges from 2.2 to 3‰, with no defined temporal trend (Figure 3). In core 13MC (2503 m), both species show a relatively abrupt decrease from glacial (2.5–3.5‰) to interglacial (1–1.5‰) values, but this shift occurs substantially shallower (5–10 cm) than the corresponding shift in benthic and *N. incompta* $\delta^{18}O$ values (25–35 cm). In core 06MC (2688 m), the two species show an intermediate depth minimum around 10–15 cm, where the $\delta^{18}O$ values decrease by more than 1‰ from 2.5–to 3‰ to 1–1.5‰ (Figure 2). No corresponding $\delta^{18}O$ shift is observed in the benthic $\delta^{18}O$ records in this sediment interval. *G. bulloides* then returns to the deeper, higher $\delta^{18}O$ values (2.5–3‰) in the coretop, but the absence of *N. pachyderma* in this interval prevents secondary confirmation of this trend. Core 10MC (2711 m) is at an almost equivalent water column depth as 06MC, but it contains a temporal trend more similar to 13MC than to 06MC. Both *G. bulloides* and *N. pachyderma* show glacial values (2.5–3.0‰) in deeper sediments, and *G. bulloides* shows some indication of interglacial values (1–1.5‰) near the core top. Again this shift to interglacial values occurs shallower (10–20 cm) than the corresponding shift in benthic and *N. incompta* $\delta^{18}O$ values (25–30 cm). The deepest core, 23TC (2906 m), is the only one to demonstrate any temporal coherence between *G. bulloides* and *N. pachyderma* and the benthic species. The planktonic species show a decrease from glacial type values (2.5–3.5‰) to interglacial type values (1–2‰). This transition (5–20 cm) starts later than the corresponding shift in the benthics (10–40 cm), but it at least overlaps the same interval.

Radiocarbon Ages

The ages derived from ^{14}C dating generally increase with increasing depth in the sediment core, with the youngest age (~50 yr) occurring at 5 cm depth (13MC) and the oldest age (~32 ka) occurring at 39 cm depth (53MC) (Table 1, Figure 5). However, this overall pattern is not manifested as the characteristic monotonic increase in age with depth. Instead, nearly all cores show a plateau region with multiple depths returning the same age. For *N. incompta*, this plateau occurs ~2–2.5 ka from 5–30 cm composite depth, while for *G. bulloides* this plateau occurs ~15–16 ka from 12–35 cm composite depth. These plateaus occur simultaneously in the depth domain within each core, suggesting a nearly 12,000-yr difference in age between foraminiferal species found within the same sedimentary horizon.

In sediment older than the plateau age, a more typical trend of increasing age with depth develops in *G. bulloides* (Figure 5). In 23TC, this trend suggests a sedimentation rate of 3.93 cm/kyr, which is about three times greater than the sedimentation rate calculated at 53MC (1.23 cm/kyr), although both are generally consistent with the range of sedimentation rates previously observed in the piston cores from this location (Costa et al. 2016). Higher sedimentation rates at 23TC are not unexpected given its location within a bathymetric low where sediment focusing would preferentially accumulate material. When the ^{14}C-based ages are adjusted onto the composite depth scale, the cores give almost identical sedimentation rates (1.23 cm/kyr at 53MC and 1.29 cm/kyr at 23TC; Figure 5, 35–50 cm composite depth).

Age Model

Because of the irreconcilable differences between the ^{14}C results from the two foraminiferal species, a direct generation of a ^{14}C-based age model is not straightforward. There is no a priori justification for trusting the *N. incompta* ages over the *G. bulloides* ages, or vice versa. Instead, a range of different ^{14}C-based age models were applied to the composite *Uvigerina* sp. $\delta^{18}O$

https://doi.org/10.1017/RDC.2017.91 Published online by Cambridge University Press

Table 1 Samples analyzed for radiocarbon ages, presented as reservoir corrected calendar ages.

Core	Sample depth (cm)	*G. bulloides* calendar age (yrs)	±	*N. incompta* calendar age (yrs)	±
06MC	21			2269	113
06MC	24	13911	193		
06MC	27	13765	224		
06MC	31	14296	212		
10MC	17			2016	98
10MC	24	15778	190		
10MC	30	15272	217		
10MC	39	18134	223		
13MC	5	1010	89	47	47
13MC	13	14968	209	2644	115
13MC	20	15048	211	1394	64
13MC	27	15401	189	2905	87
13MC	35	16399	199		
23TC	19	14563	351		
23TC	28	15402	181		
23TC	44	16399	199		
23TC	66	21994	273		
53MC	1	13843	215		
53MC	7	19391	310		
53MC	13	19250	295		
53MC	20	16719	153		
53MC	29	23684	260		
53MC	39	32215	721		

record to construct the best fit correspondence with other deglacial $\delta^{18}O$ records from the Northeast Pacific (Karlin et al. 1992; McDonald 1993; Brunelle et al. 2010; Praetorius et al. 2015).

Utilizing monospecific ^{14}C results defines two endmember age models (Figure 6). The first incorporates only the *N. incompta* ages for the top 20 cm, and then it transitions to the *G. bulloides* ages when *N. incompta* ages are no longer available (Figure 6A). This age-versus-depth evolution would require an extreme shift in sedimentation rates at 2.9 ka from 0.94 cm/kyr to 7.79 cm/kyr. The resulting isotopic record contains a deglacial transition in *Uvigerina* sp. $\delta^{18}O$ that occurs much too late compared to the regional records, starting at ~10 ka and reaching interglacial type $\delta^{18}O$ only at the very core top. The second endmember age model employs only the *G. bulloides* dates (Figure 6C), and it requires two extreme shifts in sedimentation rates: from 1.20 cm/kyr to 10.5 cm/kyr at 16 ka and then from 10.5 cm/kyr back down to 0.64 cm/kyr at 14 ka. The resulting $\delta^{18}O$ record includes a deglacial transition that occurs too abruptly at ~15 ka relative to the other regional records.

Instead we find that an intermediate age model provides the best fit of the composite *Uvigerina* sp. $\delta^{18}O$ record to the regional $\delta^{18}O$ records (Figure 6B). This age model also eliminates the necessity of an abrupt or extreme change in sedimentation rate, with a relatively modest increase from 0.93 cm/kyr to 1.80 cm/kyr at 22.5 ka. These sedimentation rates are within the limits observed within the piston cores from this region (Costa et al. 2016). However, this best fit

https://doi.org/10.1017/RDC.2017.91 Published online by Cambridge University Press

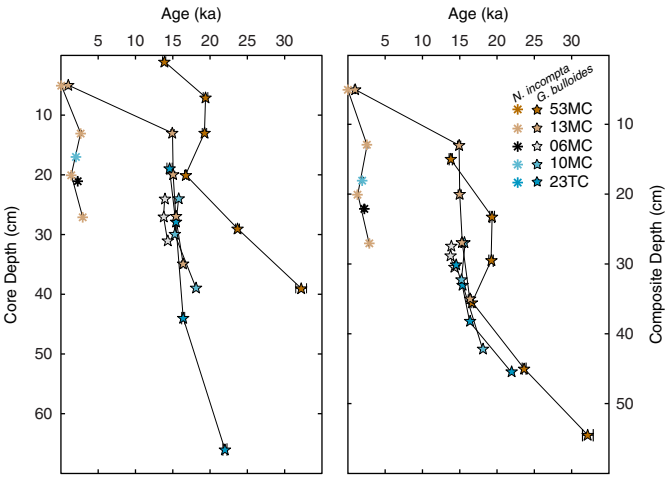

Figure 5 ^{14}C-based ages versus depth profiles for the five sediment cores. All ages are presented as calendar years. Legend applies to both panels, with data shown on individual core depths on the left and composite depth (see Figure 3) on the right.

age model does imply that in fact neither the *G. bulloides* nor the *N. incompta* ^{14}C ages reflect the actual age of the sediment. This presents the conundrum of how to explain, for example, the simultaneous 2 ka age of *N. incompta*, 6 ka of the sediment, and 15 ka age of *G. bulloides*.

Total Particle Flux

The ^{230}Th based total particle fluxes show a coherent pattern of maximum values during the last glacial period and minimum values during the Holocene across all five cores (Figure 7, left). The last glacial period averages 1.35 g/cm^2 kyr, while the average Holocene flux is nearly 2/3 lower at just 0.51 g/cm^2 kyr. Fluxes are highest at the shallowest core, 53MC, and lowest at the deepest core, 23TC. This trend is most readily apparent in the Holocene, with particle flux decreasing from 0.75 g/cm^2 kyr at 53MC (2347 m), 0.60 g/cm^2 kyr at 13MC (2503 m), 0.43 g/cm^2 kyr at 10MC (2711 m), and 0.40 g/cm^2 kyr at 23TC (2906 m). The transition from the high particle flux glacial period into the low particle flux Holocene occurs fairly abruptly, but it is interrupted by a brief return to higher fluxes ~15–16 ka, possibly reflecting the expected deglacial maximum in $CaCO_3$ preservation (Mekik et al. 2012).

All cores display an increase in sediment focusing over the past 30 kyr, with the exception of 23TC, although uncertainties in the age models create large error envelopes (Figure 7, right). Sediment focusing peaks in core 23TC ($\Psi = 2.67$) during the early deglaciation (15–20 ka), and then focusing gradually decreases down to unity by the late Holocene. With the exception of 06MC, average sediment focusing over the full 30 kyr period is inversely dependent on water depth: $\Psi = 0.73$ at 53MC (2347 m), $\Psi = 1.01$ at 13MC (2503 m), $\Psi = 1.47$ at 10MC (2711 m), and $\Psi = 1.53$ at 23TC (2906 m). Core 06MC contains anomalously high sediment focusing ($\Psi = 2.11$ on average) for its water depth (compared to 10MC), but this feature is consistent with increasing sediment focusing observed near the coretop of the corresponding piston core, AT26-19-09PC (Costa and McManus 2017), indicating a localized sediment focusing effect. All multicores that reach the last glacial period show winnowing at that time in this mid-latitude study area, in contrast to evidence that suggests that high sediment focusing may have characterized

https://doi.org/10.1017/RDC.2017.91 Published online by Cambridge University Press

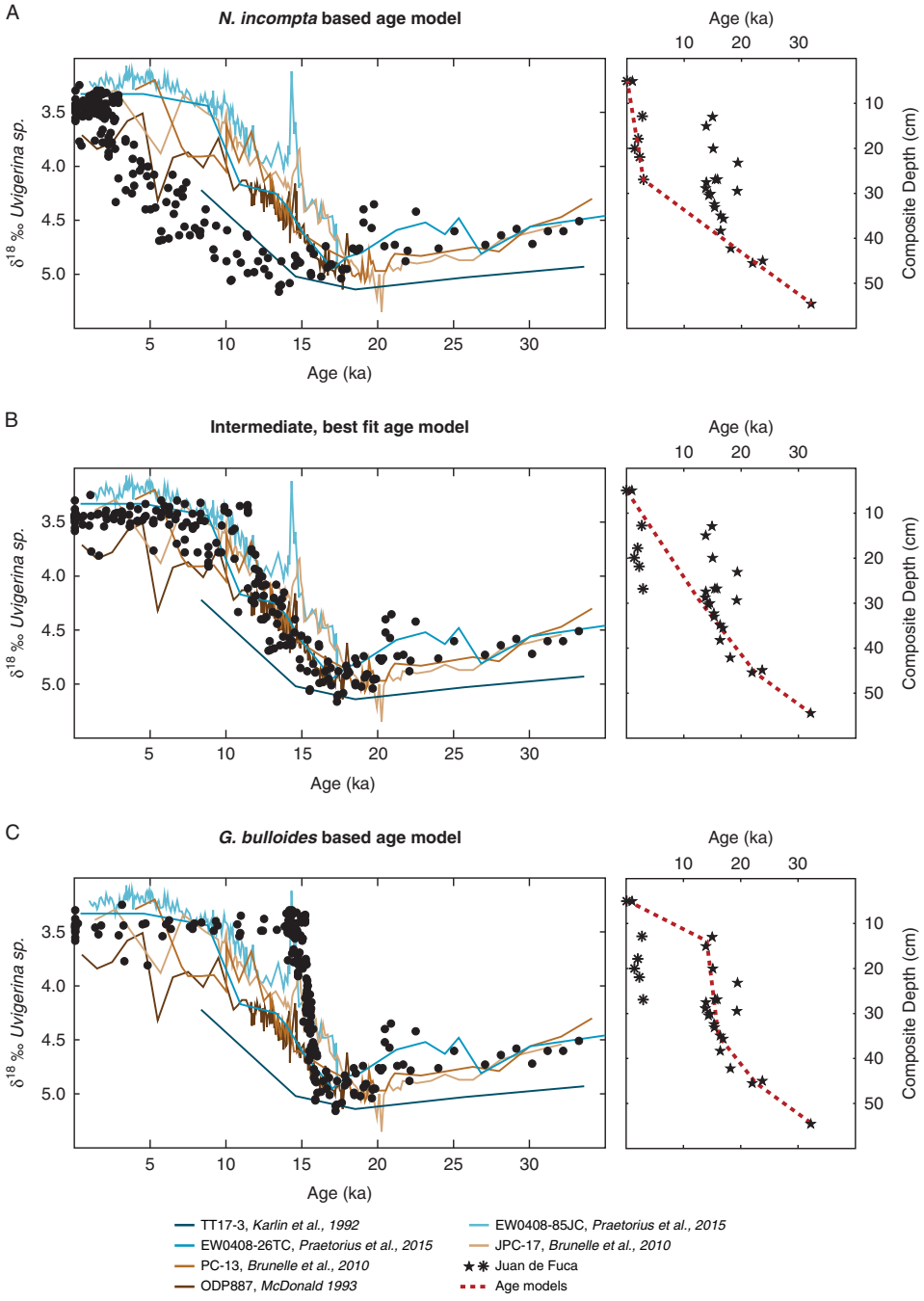

Figure 6 Age model generation. Right panels present ^{14}C data from *G. bulloides* (stars) and *N. incompta* (asterisks), as in Figure 4, with age models identified by dashed red lines. All ages are presented as calendar years, and depths are composite depth, as in Figure 3. Left panels show the results of applying the various age models to the composite $\delta^{18}O$ of *Uvigerina* sp. from the JdFR (black dots). The resulting progression of $\delta^{18}O$ with age was compared with that of other regional records (Karlin et al. 1992; McDonald 1993; Brunelle et al. 2010; Praetorius et al. 2015) in order to evaluate the success of each age model.

https://doi.org/10.1017/RDC.2017.91 Published online by Cambridge University Press

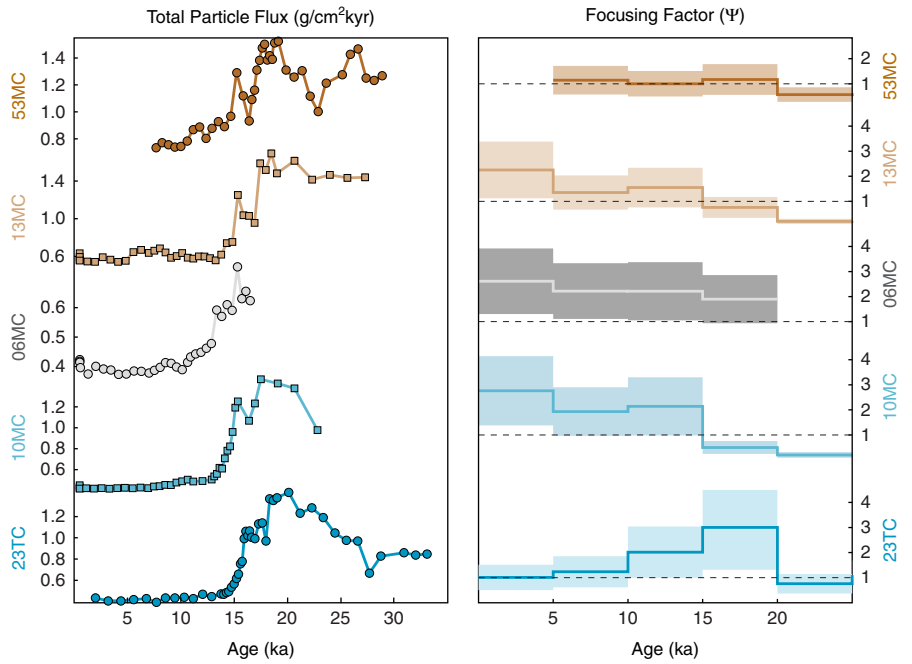

Figure 7 Total particle fluxes (left) and focusing factors (right). Total particle fluxes decrease by about 2/3 from the LGM to the Holocene, and Holocene fluxes are water depth dependent with the highest fluxes at 53MC and the lowest fluxes at 23TC. Error bars show 2σ when larger than symbol size. Focusing factors record the relative input of laterally redistributed sediment. Values greater than 1 indicate sediment focusing, or substantial lateral contributions of sediment. Values less than 1 indicate sediment winnowing, or post-depositional removal of sediment. Shaded regions show the error envelopes assuming a conservative estimate of 50% error in the age assignment.

glacial sediment deposition in the Equatorial Pacific (Marcantonio et al. 2001; Higgins et al. 2002; Kienast et al. 2007; Mitchell and Huthnance 2013).

DISCUSSION

Without sediment mixing, age versus depth profiles should reflect a monotonic increase with depth at a slope equivalent to the mean sedimentation rate. Bioturbation interrupts this trend by homogenizing a range of sedimentary horizons into a single unit, which can create an age plateau in the surface mixed layer. Besides bioturbation, there are many non-chronological processes that may also influence ^{14}C ages (Mekik 2014), especially in low sedimentation rate sites like the JdFR. Chemical erosion (Keir 1984), interface dissolution (Broecker et al. 1991; Keir and Michel 1993), and secondary calcification in the sediment (Broecker et al. 1984, 1990, 2000, 2006; Barker et al. 2007) may bias all foraminiferal ^{14}C dates simultaneously, regardless of species. Habitat depth differences (Waelbroeck et al. 2001), abundance variations (Manighetti et al. 1995; Barker et al. 2007), differential dissolution and fragmentation (Barker et al. 2007), degree of ontogenetic encrustation (Kozdon et al. 2009), sediment remobilization (Broecker et al. 2006; Barker et al. 2007), and morphologically dependent bioturbation (Peng and Broecker 1984) can dissociate ^{14}C ages of different species within the same sediment interval. Age offsets between foraminiferal species are generally no more than 1–3 kyr, but larger ^{14}C offsets on the order of 10 kyr have been observed between alkenones and

https://doi.org/10.1017/RDC.2017.91 Published online by Cambridge University Press

foraminifera (Ohkouchi et al. 2002; Mollenhauer et al. 2003, 2005, 2006, 2011; Uchida et al. 2005), between foraminiferal species within extremely bioturbated zoophycos channels (Löwemark and Werner 2001; Leuschner et al. 2002; Löwemark and Grootes 2004), and between frosty and glassy tests of variably preserved foraminifera of the same species (Wycech et al. 2016).

On the JdFR, the ~12 kyr offset between *N. incompta* and *G. bulloides* in the upper 30 cm coincides with simultaneous age plateaus in each species: nearly all the *N. incompta* ages are between 2–3 ka while all but the shallowest *G. bulloides* ages are 15–16 ka. The severe age discrepancy combined with this age plateau may eliminate some of the aforementioned discriminating processes as improbable. In even the most extreme habitat comparison, planktic versus benthic, ^{14}C differences between foraminiferal species only achieve 3 kyr offsets at most (Broecker et al. 1984; Keigwin and Schlegel 2002; Skinner and Shackleton 2004; Barker et al. 2007; Lund et al. 2011). Ontogenetic encrustation in one species but not the other could cause an age offset but would be unlikely to return constant ages over such a large depth range, and the nearly identical average shell weights for the two species (12.2 µg for *G. bulloides* and 12.1 µg for *N. incompta*) may not be consistent (Lohmann 1995; Broecker and Clark 2001) with this process favoring only one species (supplementary Figure 3). Preferential remobilization and bioturbation of the more rounded *G. bulloides* tests may contribute to the age plateau in that species (Figure 5, 5–30 cm composite depth), but a preference for *G. bulloides* would not explain why the same outcome at a different age is observed in the *N. incompta* data as well (Figure 5, 10–40 cm composite depth). Similarly, *G. bulloides* may be more susceptible to partial dissolution than *N. incompta* (Berger 1970), which may contribute to the older ages for *G. bulloides* (Wycech et al. 2016) and the relatively constant age offset between *N. incompta* and *G. bulloides,* but the age plateau would require an anomalously large mixing depth of ~30 cm, considerably deeper than the global average 6–16 cm (Broecker et al. 1991). Although these processes may contribute an ancillary influence on the age offset and age plateaus, the probability of manifesting these features is greatly increased when changes in foraminiferal assemblage and concentration, specifically an abundance peak of *N. incompta* at 2.5 ka and *G. bulloides* at 15–18 ka, are also considered (Ruddiman et al. 1980; Ruddiman and McIntyre 1981).

The relatively young age plateau in *N. incompta* around 2.5 ka is consistent with its increasing dominance of the planktic foraminiferal pool at shallower sediment depths. This shift towards *N. incompta* during the Holocene reflects its preferred habitat for relatively warmer waters than its other subpolar counterparts (Be and Tolderlund 1971; Coulbourn et al. 1980; Žarić et al. 2005; Darling and Wade 2008). In a spatial assessment of modern coretops from the North Atlantic, the sediment assemblage shifts from *N. pachyderma* dominated to *N. incompta* dominated south of the 7.2ºC isotherm (Ericson 1959; Pflaumann et al. 2003). A similar shift in assemblage is observed in response to warming temperatures during the deglaciation in the Northeast Pacific, with declining abundance of *N. pachyderma* in the coretop sediment coincident with the development of a more favorable habitat for *N. incompta* (Figure 3). The young age for the *N. incompta* plateau may be associated with the local maxima in absolute abundance around 12–15 cm, which has likely been bioturbated up and down the core. *G. bulloides*, unlike *N. incompta*, can thrive under a much wider range of environmental conditions (Be and Tolderlund 1971; McManus et al. 1998, 1999; Oppo et al. 1998; Pflaumann et al. 2003; Darling and Wade 2008), as evidenced by its sustained abundance in all but the very core top samples. The transition from glacial to interglacial climate does not spontaneously optimize the growth conditions for *G. bulloides*, and the concentration only begins to drop off in the late Holocene when corrosive bottom waters more insistently dissolve the rather fragile *G. bulloides* tests

https://doi.org/10.1017/RDC.2017.91 Published online by Cambridge University Press

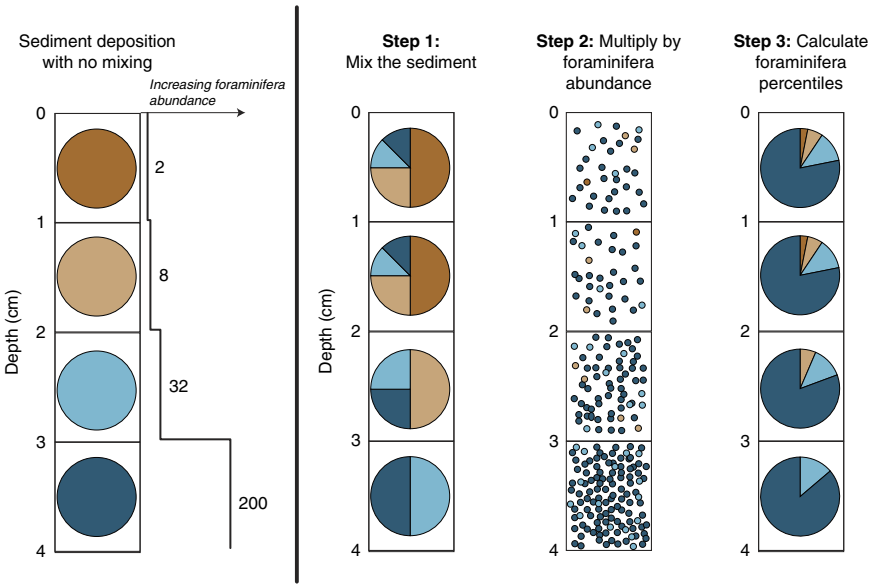

Figure 8 Schematic example of the sediment mixing model. Consider 4 cm of sediment composed of four 1-cm layers with decreasing foraminiferal abundance over time. With no sediment mixing, each sediment layer will contain 100% of its original sediment deposited during that time interval. The change in foraminiferal abundance (two orders of magnitude) is similar to that observed for *N. pachyderma* in the Juan de Fuca cores. In Step 1, the sediment is mixed assuming complete mixture in a 2 cm mixed layer from the bottom to the top. For example, after mixing, the sedimentary layer from 2–3 cm contains 50% sediment originally from 1–2 cm (light orange), 25% of its own original sediment (2–3 cm, light blue), and 25% sediment originally from 3–4 cm (dark blue). In Step 2, the sediment distributions determined at the end of Step 1 are multiplied by the foraminiferal abundance in each of those sedimentary units to determine the number of foraminifera (circles) contributed by each layer. For example, the sedimentary layer from 2–3 cm contains 4 foraminiferal tests from 1–2 cm (light orange), 8 foraminiferal tests from 2–3 cm (light blue), and 50 foraminiferal tests originally from 3–4 cm (dark blue). In Step 3, the foraminiferal assemblage from Step 2 is divided by the total number of foraminifera in each layer in order to generate foraminiferal percentiles. For example, the foraminifera in the 2–3 cm layer originate 6.5% from 1–2 cm (light orange), 12.9% from 2–3 cm (light blue), and 80.6% from 3–4 cm (dark blue). The persistently abundant foraminifera from 3–4 cm (dark blue) easily overwhelm the younger foraminifera, and they demonstrate how an age plateau may arise as a result of changes in abundance. (Colors refer to online version.)

(Berger 1970). Peaks in *G. bulloides* flux at ~15 ka (30 cm) and ~18 ka (35 cm) occur simultaneously with peaks in both *N. pachyderma* and *N. incompta*, suggesting an increase in carbonate preservation at these times (Mekik et al. 2012) rather than particularly favorable conditions for *G. bulloides* alone. However the sheer magnitude of the ~18 ka (35 cm) abundance peak, nearly double the average flux of the last glacial period and over 1000× the flux of the Holocene (Figure 3, left), suggests that bioturbation of this peak has contributed to the relatively old age plateau ~15 ka in *G. bulloides.*

Sediment Mixing Model

To assess the evolution of sediment mixing over the past 30 kyr, an iterative mixing model was designed and optimized to the results previously described. The model focuses on core 13MC from which the greatest number of ^{14}C dates ($n = 9$) is available and for which full

https://doi.org/10.1017/RDC.2017.91 Published online by Cambridge University Press

assemblage counts were conducted. The first step of the model is to mix the sediment units over a mixed layer depth parameterized as a Tukey window (Figure 8, Step 1). A sediment unit is deposited with the initial conditions of 100% contemporaneous sediment (e.g., the 15 cm sediment unit contains 100% sediment from 15 cm), and after mixing, each unit contains a spectrum of different sedimentary units (e.g., the 15 cm sediment unit may contain 10% sediment originally from 35 cm). This process is repeated with each new sedimentary layer until the top of the sediment core is reached, generating a matrix of varying sediment assemblages with depth.

The sediment assemblage is then converted to a foraminiferal assemblage by correcting for the density and foraminiferal concentration differences between sedimentary layers (Figure 8, Step 2). Sediment density generally decreases from glacial to interglacial periods (Costa et al. 2016), and so sediment from deeper (glacial) sediment layers will contain more mass than sediment from shallower (interglacial) layers. Foraminiferal concentrations similarly decrease from glacial to interglacial samples (Figure 3). The model utilizes the (post-mixing) foraminiferal concentrations as depicted in Figure 4, without performing any manipulations to reconstruct the pre-mixing concentrations. While the calculated concentrations in Figure 4 represent the abundances post-mixing, the model uses them with the assumption that these concentrations would be proportional to the concentrations that would characterize the initial sediment unit pre-mixing. For example, if 10% of the sediment in an interval comes from 15 cm depth, which has a foraminiferal concentration of 100 specimens/g, then 10 specimens within that interval originated in the 15 cm sediment unit. The individual contributions of each sediment fraction could then be summed and divided by that sum to derive the percentile foraminiferal assemblages (Figure 8, Step 3). These percentile foraminiferal assemblages are not equivalent to the sediment assemblages but are instead heavily weighted towards the contributions from the far more abundant foraminifera within glacial sediment. For example, the 15 cm sediment unit may contain 10% sediment originally from 35 cm, but the high density and foraminiferal count in that 35 cm sediment might lead to a contribution of 30% of the foraminifera in the resulting sediment mixture. This glacial bias increases as the amplitude of the glacial-interglacial shift in foraminifera abundance increases, so that it affects *G. bulloides* more than *N. incompta.*

The model then utilizes the percentile foraminiferal assemblage for Monte Carlo simulation of the foraminifera selection (picking) process for ^{14}C and stable isotope analyses. A random sample of 300 foraminifera for ^{14}C or 10 foraminifera for stable isotopes are selected from the population and averaged to determine the resulting mean value. Age assignments for individual foraminifera were based on their original deposition interval (e.g. foraminifera from 35 cm would be 18 ka), while $\delta^{18}O$ assignments were based on the *Uvigerina* sp. $\delta^{18}O$ trend, scaled to match the range observed in each planktonic species. The random sampling process was repeated 1000 times to return the possible age and $\delta^{18}O$ distributions at each sediment depth.

The model first assessed a range of constant mixing depths from 0 to 20 cm (Figure 9). All mixing depths greater than 3 cm generated an age plateau in *G. bulloides* that ranges from 10 to 18 ka, but none recreated the particularly prolonged and stable age plateau at 15 ka over ~25 cm of sediment, as observed in the data. Shallower mixing depths (0–7 cm) are better aligned with ^{14}C data than the larger mixing depths, because the larger mixing depths sustain the abundant ~18 ka foraminifera through a greater range of the sediment column. Unfortunately, not even the 0 cm mixing depth (no mixing) simulation can recreate the very young *N. incompta* ^{14}C ages, while even a very deep (30 cm) mixed layer fails to prolong an *N. incompta* age plateau down to

https://doi.org/10.1017/RDC.2017.91 Published online by Cambridge University Press

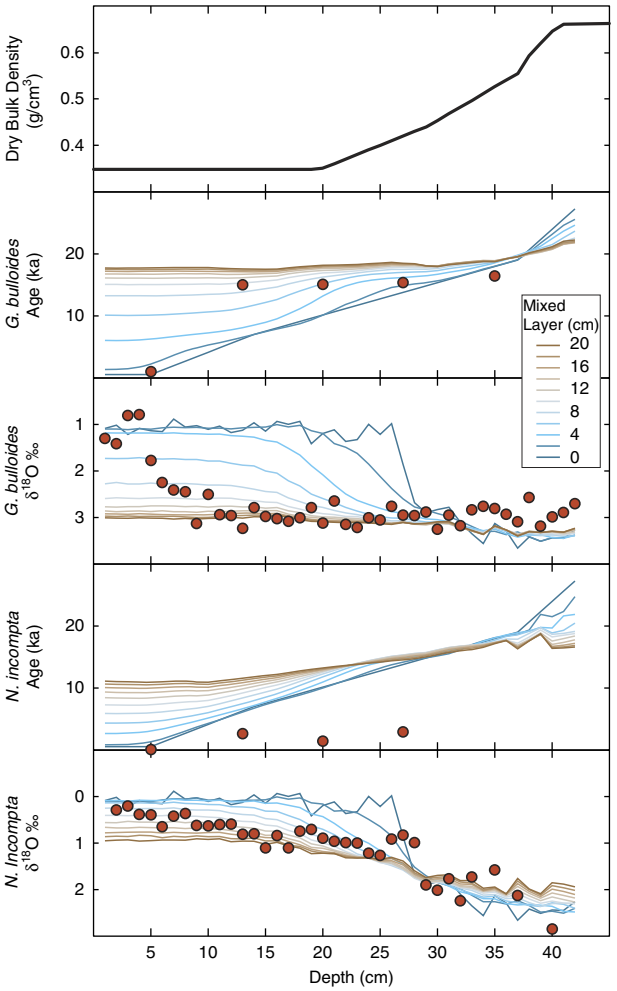

Figure 9 Simulation of foraminiferal age and $\delta^{18}O$ profiles for *G. bulloides* and *N. incompta* from core 13MC using the iterative sediment mixing model (see Sediment Mixing Model section). Dry bulk density (top panel) interpolated from previously published records of piston cores from the same region as the multicores (Costa et al. 2016). Sediment was bioturbated upwards using a Tukey window, and then foraminiferal abundances were applied to determine the range of values within the foraminiferal assemblage at each depth. Foraminifera were randomly selected ($n = 300$ for ^{14}C, $n = 10$ for $\delta^{18}O$) and averaged, and this sampling was repeated 1000 times to determine a representative value given the foraminiferal assemblage at each depth. Legend applies to all panels and identifies model output using constant mixed layers of different depths. Red dots indicate the actual data. (Color refers to online version.)

27 cm depth (supplementary Figure 4). This inconsistency between *G. bulloides* and *N. incompta* indicates that other processes in addition to the diffusive sediment mixing modeled here must be contributing the young *N. incompta* ages. In contrast to the ^{14}C results, the $\delta^{18}O$ records for *G. bulloides* and *N. incompta* instead present evidence in favor of larger mixing layers. Mixing

https://doi.org/10.1017/RDC.2017.91 Published online by Cambridge University Press

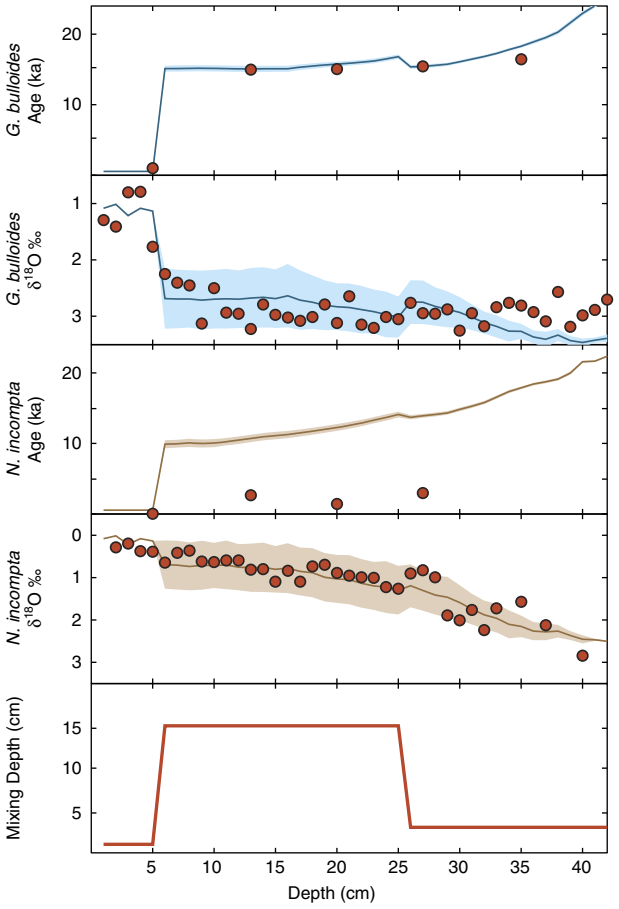

Figure 10 Optimized conditions for the iterative sediment mixing model (see Figure 8 and Sediment Mixing Model section). Model outputs were calculated by employing the variation in mixing depth shown in the bottom panel. Shaded envelopes define 1σ of 1000 bootstrap sampling runs for the model output, and they are much wider for $\delta^{18}O$ due to the smaller foraminiferal sample in the average ($n = 10$) compared to age ($n = 300$). Red dots indicate the actual data. The increase in mixing depth ~25 cm is necessary to prolong the 15 ka age plateau in *G. bulloides* to 13 cm depth. (Color refers to online version.)

layers that are less than 9 cm create a transition from glacial to interglacial conditions both too gradually and too early in the sediment record for both species. This disagreement between the ^{14}C and $\delta^{18}O$ records indicates that a single, constant mixing depth over the past 30 ka is improbable.

An improved fit for both the *G. bulloides* ^{14}C and both species' $\delta^{18}O$ data can be obtained when the mixing depth is allowed to vary over the course of the depositional history (Figure 10). The optimization compromises between the earlier implications from ^{14}C and $\delta^{18}O$ by starting at a relatively small mixing layer (3 cm) during the glacial period followed by an abrupt transition to a large mixing layer (13–15 cm) at 24–25 cm and then returning to small mixing layers in the

https://doi.org/10.1017/RDC.2017.91 Published online by Cambridge University Press

sediment coretop. The abrupt shift to higher mixing corresponds nominally to the early Holocene, and the timing and high magnitude are both necessary to delay the transition to interglacial values of $\delta^{18}O$ in *G. bulloides* until after 10 cm and to maintain the 15 ka age plateau in *G. bulloides* up to at least 13 cm. The transition back to low mixing depths ($\leq$2 cm) is required by no later than 5 cm in order to secure the young age (1 ka) of the *G. bulloides* at 5 cm depth. The $\delta^{18}O$ values in *N. incompta* are less sensitive to one particular mixing depth over another, but they oblige the *G. bulloides* constraints with relative consistency to the model. Overall, an excellent agreement between the model and the *G. bulloides* ages and good agreements between the model and the stable isotope records can be achieved by employing a deeper mixed layer from 5–25 cm (nominally 0.5–12.7 ka).

While this simple model parameterizes the changes in mixing as discrete mixing depth intervals, changes in mixing could also be effected by varying the mixing rates (Peng et al. 1979; Demaster and Cochran 1982; Cochran 1985). The model presented here assumes an infinite mixing rate within the mixed layer, perfectly homogenizing the sediment within that mixed layer, below which the mixing rate is zero. A more realistic transition might incorporate a depth gradient in mixing rate, and indeed more complex models of bioturbation may sometimes employ multiple mixed layers characterized by variable mixing rates (e.g., Benninger et al. 1979). The increase in mixing depth that emerges in the model used in this study could alternatively be interpreted as an equivalent increase in mixing rates, or a smaller increase in both mixing rate and mixing depth. Regardless, the model is capable of demonstrating how a change in mixing parameters can generate the particular nuances of the JdFR data, including the prolonged and stable age plateau in ^{14}C as well as the delayed transition to interglacial $\delta^{18}O$ values. Considering the limitations of the model, we therefore prefer the more generalized interpretation of the results as an increase in mixing "intensity" rather than specifically in terms of mixing depth.

Increased mixing intensity in the Holocene may not be inconsistent with *N. incompta* ages if secondary processes are also considered. In particular, underestimation of the coretop abundance of *N. incompta* may largely explain the model's failure to reconstruct the young *N. incompta* age plateau. The model parameterizes the *N. incompta* abundance after the post-mixing concentrations counted in the sediment (Figure 4H), in which coretop abundances (0.4 specimens/g) are two orders of magnitude lower than the maximum abundances (40 specimens/g) at depth. If instead the coretop abundance (0–5 cm) were 300–500 × greater, a deep mixing layer in the Holocene would indeed recreate the young *N. incompta* age plateau (supplementary Figure 5). This hypothetical evolution in *N. incompta* absolute abundance would mirror that of its relative abundance (Figure 4G), in which *N. incompta* becomes more dominant in the Holocene due to a more favorable (i.e., warmer) surface environment. Underestimation of the *N. incompta* abundance may be a result of preferential dissolution of the younger tests, while secondary precipitation of that calcite onto older *N. incompta* tests would retain the young ^{14}C signature in the species. Why this mechanism would apply to *N. incompta* but not *G. bulloides* is unclear. Regardless, such a mechanism would imply the testable hypothesis that leached *N. incompta* tests from depth would return older ages, and the ongoing development of small sample size ^{14}C analyses (Bush et al. 2013) may make this assessment feasible in the near future.

Possible Drivers of Changes in Mixing Intensity over the Last 30 kyr

A shift towards more intense sediment mixing in the Holocene suggests a corresponding amelioration of environmental conditions previously limiting mixing in the glacial period. This interval corresponds with a slight decrease in sediment focusing, at least in core 13MC, and

https://doi.org/10.1017/RDC.2017.91 Published online by Cambridge University Press

terminates with a near doubling of sediment focusing at 5 ka. Sediment mixing intensity may be obscured by inverse changes in sedimentation rates, and a sudden increase in the lateral influx of sediment would require an increase in the mixing intensity in order to maintain the same level of temporal homogeneity of the sediment. For example, an 8 cm mixing depth of sediment that accumulates at 1 cm/kyr would result in sediment with an average age of ~3 ka. If that 8 cm mixing depth persisted as accumulation rates increased to 2 cm/kyr, then the average age of the sediment in the mixed layer would only be 1.4 ka. Without knowledge of changes in sediment influx, this shift in the mixed layer could instead be inferred as a decrease in the mixing depth from 8 cm to 4 cm. Thus, the decrease in mixing intensity inferred in the late Holocene may be partly a result of the increase in sediment focusing and sediment influx at this time, although further mechanisms are likely required to explain the large amplitude.

The benthic community may have provided the extra boost in sediment mixing from enhanced bioturbation in response to increased oxygen conditions. An increase in deepwater oxygen concentrations might increase the mixing by allowing aerobic heterotrophs to overturn deeper stratigraphic layers of sediment in search for food. Previous studies have identified hypoxic (low-oxygen) events during the Bolling-Allerod (15 ka) across the North Pacific (Zheng et al. 2000; Crusius et al. 2004; Cook et al. 2005; Jaccard and Galbraith 2012; Lam et al. 2013; Rae et al. 2014; Praetorius et al. 2015) generally associated with a peak in productivity (Kohfeld and Chase 2011), but observations during the Holocene are sparse and somewhat contradictory. In the Gulf of Alaska, shallow water depths (<400 m) experience hypoxic events in the Bolling-Allerod and in the early Holocene, but deeper sites (<2000 m) demonstrate similarly oxygenated glacial and Holocene sediment (Praetorius et al. 2015). Relatively shallow waters (800 m) along the California Coast suggest oxygen levels may have been slightly lower in the Holocene than in the glacial period (Zheng et al. 2000), but deep waters (3300 m) in the Northwest Pacific show oxygen concentrations equal to or greater than that of the glacial period (Lam et al. 2013). Intermediate waters in the Northeast Pacific do not show a clear difference between oxygen conditions in the glacial period (20–22 ka) compared to the Early Holocene (5–10 ka) (Jaccard and Galbraith 2012), when the model would predict the greatest change in mixing intensity.

Oxygen concentrations may be affected by changes in the circulation regime. The JdFR currently resides below the North Pacific oxygen minimum zone, with oxygen concentrations increasing with water depth from as low as 17.5 μmol at 1000 m water depth to 90–100 μmol/L at the core sites (2300–2900 m) (World Ocean Atlas 2013). If the oxygen minimum zone deepened to intersect the JdFR, it would enforce the low oxygen concentrations on the benthic ecology and stifle sediment mixing, but it is unclear why the oxygen minimum zone would have then shoaled in the Holocene. Alternatively, oxygen concentrations in deepwater may vary in response to transit time from the Southern Ocean northward. Relatively younger water masses would retain greater oxygen concentrations as they would experience relatively lower levels of net respiration. Studies of benthic-planktic ^{14}C differences have found substantial changes in ventilation age of North Pacific bottom waters during the deglaciation (Okazaki et al. 2010; Lund et al. 2011; Rae et al. 2014), but few data are available to track changes in ventilation within the Holocene interval. Future work reconstructing oxygen concentrations across the North Pacific throughout the Holocene may be necessary to confirm whether variations in deep circulation can account for the changes in mixing intensity proposed here over the last 30 kyr.

CONCLUSIONS

Sediment mixing is omnipresent throughout the global ocean but poorly constrained beyond the observation and modeling of modern sedimentary mixed layers. Because sediment mixing

https://doi.org/10.1017/RDC.2017.91 Published online by Cambridge University Press

can respond to environmental parameters, it is likely to have varied in the past under different paleoceanographic and paleoclimatic conditions. Here, diverging ^{14}C and oxygen isotopic records from two species, *G. bulloides* and *N. incompta*, at five study sites in the Northeast Pacific provide evidence for substantial changes in sediment mixing since the last ice age. These records indicate that mixing intensity increased during the early Holocene after a period of relatively weaker mixing in the glacial period. The early Holocene shift may have occurred in response to increasing bottom water oxygen concentrations during this time, possibly related to a change in ventilation, although records of oxygen concentrations during the Holocene are currently inconclusive. Changes in the extent of sediment mixing have the greatest influence on the $\delta^{18}O$ and ^{14}C of planktonic foraminifera species that vary dramatically in abundance during the study interval. Despite the observed changes in mixing, substantial age control is nevertheless provided by benthic $\delta^{18}O$ so that a reliable chronology for these cores can still be constructed.

ACKNOWLEDGMENTS

The authors thank Wei Huang, Nicholas Mehmel, and Grace Cushman for assistance with $\delta^{18}O$ sample processing and analysis at LDEO. The data are archived on the NOAA paleoclimate database. This research was funded by NSF-AGS-#1338832 to JFM and a NSF Graduate Research Fellowship to KMC.

SUPPLEMENTARY MATERIAL

To view supplementary material for this article, please visit https://doi.org/10.1017/RDC.2017.91

REFERENCES

Anderson DM. 2001. Attenuation of millennial-scale events by bioturbation in marine sediments. *Paleoceanography* 16(4):352–7. DOI: 10.1029/2000PA000530.

Bacon MP. 1984. Glacial to interglacial changes in carbonate and clay sedimentation in the Atlantic Ocean estimated from ^{230}Th measurements. *Isotope Geoscience* 2:97–111.

Bard E, Arnold M, Duprat J, Moyes J, Duplessy J-C. 1987. Reconstruction of the last deglaciation: deconvolved records of $\delta^{18}O$ profiles, micropaleontological variations, and accelerator mass spectrometric ^{14}C dating. *Climate Dynamics* 1:101–12.

Barker S, Broecker W, Clark E, Hajdas I. 2007. Radiocarbon age offsets of foraminifera resulting from differential dissolution and fragmentation within the sedidmentary bioturbated zone. *Paleoceanography* 22(2):1–11. DOI: 10.1029/2006PA001354.

Behl RJ, Kennett JP. 1996. Brief interstadial events in the Santa Barbara basin, NE Pacific, during the past 60 kyr. *Nature* 379(6562):243–6. DOI: 10.1038/379243a0.

Bemis BE, Spero HJ, Bijma J, Lea W. 1998. Reevaluation of the oxygen isotopic composition of planktonic foraminifera: experimental results and revised paleotemperature equations. *Paleoceanography* 13(2):150–60.

Benninger LK, Aller RC, Cochran JK, Turekian KK. 1979. Effects of biological sediment mixing on the ^{210}Pb chronology and trace metal distribution in a Long Island Sound sediment core. *Earth and Planetary Science Letters* 43:241–59.

Berger WH. 1970. Planktonic foraminifera: selective solution and the lysocline. *Marine Geology* 8: 111–38.

Berger WH, Heath GR. 1968. Vertical mixing in pelagic sediments. *Journal of Marine Research* 26(2):134–43.

Berger WH, Johnson RF. 1978. On the thickness and the ^{14}C age of the mixed layer in deep-sea carbonates. *Earth and Planetary Science Letters* 41(2):223–7 DOI: 10.1016/0012-821X(78)90012-2.

Boudreau BP. 1994. Is burial velocity a master parameter for bioturbation? *Geochimica et Cosmochimica Acta* 58(4):1243–9.

Broecker W, Clark E. 2001. An evaluation of Lohmann's foraminifera weight dissolution index. *Paleoceanography* 16(5):531–4.

Broecker W, Mix A, Andree M, Oeschger H. 1984. Radiocarbon measurements on coexisting benthic and planktic foraminifera shells: potential for reconstructing ocean ventilation times over the past 20,000 years. *Nuclear Instruments and Methods in Physics Research B* 5(2):331–9. DOI: 10.1016/0168-583X(84)90538-X.

Broecker W, Barker S, Clark E, Hajdas I, Bonani G. 2006. Anomalous radiocarbon ages for foraminifera shells. *Paleoceanography* 21(2):1–5. DOI: 10.1029/2005PA001212.

Broecker WS, Klas M, Clark E, Trumbore S, Bonani G, Wolfli W, Ivy S. 1990. Accelerator mass spectrometric radiocarbon measurements on foraminifera shells from deep-sea cores. *Radiocarbon* 32(2):119–33.

Broecker WS, Klas M, Clark E, Bonani G, Ivy S, Wolfli W. 1991. The influence of $CaCO_3$ dissolution on core top radiocarbon ages for deep-sea sediments. *Paleoceanography* 6(5):593–608 DOI: 10.1029/91PA01768.

Broecker WS, Clark E, Lynch-Stieglitz J, Beck W, Stott LD, Hajdas I, Bonani G. 2000. Late glacial diatome accumuation at 9°S in the Indian Ocean. *Paleoceanography* 15:348–52.

Brunelle BG, Sigman DM, Jaccard SL, Keigwin LD, Plessen B, Schettler G, Cook MS, Haug GH. 2010. Glacial/interglacial changes in nutrient supply and stratification in the western subarctic North Pacific since the penultimate glacial maximum. *Quaternary Science Reviews* 29(19–20):2579–90. DOI: 10.1016/j.quascirev.2010.03.010.

Bush SL, Santos GM, Xu X, Southon JR, Thiagarajan N, Hines SK, Adkins JF. 2013. Simple, rapid, and cost effective: a screening method for ^{14}C analysis of small carbonate samples. *Radiocarbon* 55(2):631–40.

Cheng H. et al. 2013. Improvements in ^{230}Th dating, ^{230}Th and ^{234}U half-life values, and U-Th isotopic measurements by multi-collector inductively coupled plasma mass spectrometry. *Earth and Planetary Science Letters* 371–372:82–91. DOI: 10.1016/j.epsl.2013.04.006.

Cochran JK. 1985. Particle mixing rates in sediments of the eastern equatorial Pacific: evidence from ^{210}Pb, $^{239,240}Pu$ and ^{137}Cs distributions at MANOP sites. *Geochimica et Cosmochimica Acta* 49(1982):1195–210.

Cook MS, Keigwin LD, Sancetta CA. 2005. The deglacial history of surface and intermediate water of the Bering Sea. *Deep Sea Research II* 52:2163–73. DOI: 10.1016/j.dsr2.2005.07.004.

Costa K, McManus J. 2017. Efficacy of ^{230}Th normalization in sediments from the Juan de Fuca Ridge, northeast Pacific Ocean. *Geochimica et Cosmochimica Acta* 197:215–25. DOI: 10.1016/j.gca.2016.10.034.

Costa KM, McManus JF, Boulahanis B, Carbotte SM, Winckler G, Huybers P, Langmuir CH. 2016. Sedimentation, stratigraphy and physical properties of sediment on the Juan de Fuca Ridge. *Marine Geology* 380:163–73.

Coulbourn WT, Parker FL, Berger WH. 1980. Faunal and solution patterns of planktonic foraminifera in surface sediments of the North Pacific. *Marine Micropaleontology* 5:329–99.

Crusius J, Pedersen TF, Kienast S, Keigwin L, Labeyrie L. 2004. Influence of northwest Pacific productivity on North Pacific Intermediate Water oxygen concentrations during the Bolling-Allerod interval (14.7–12.9 ka). *Geology* 32(7):633–6. DOI: 10.1130/G20508.1.

Darling KF, Wade CM. 2008. The genetic diversity of planktic foraminifera and the global distribution of ribosomal RNA genotypes. *Marine Micropaleontology* 67(3–4):216–38. DOI: 10.1016/j.marmicro.2008.01.009.

Davies MH, Mix AC, Stoner JS, Addison JA, Jaeger J, Finney B, Wiest J. 2011. The deglacial transition on the southeastern Alaska Margin: meltwater input, sea level rise, marine productivity, and sedimentary anoxia. *Paleoceanography* 26(2):1–18. DOI: 10.1029/2010PA002051.

Demaster DJ, Cochran JK. 1982. Particle mixing rates in deep-sea sediments determined from excess ^{210}Pb and ^{32}Si profiles. *Earth and Planetary Science Letters* 61:257–71.

Erez J. 1978. Vital effect on stable-isotope composition seen in foraminifera and coral skeletons. *Nature* 273 (5659):199–202. DOI: 10.1038/273199a0.

Ericson DB. 1959. Coiling direction of Globigerina pachyderma as a climatic index. *Science* 130 (3369):219–20.

Ezard THG, Edgar KM, Hull PM. 2015. Environmental and biological controls on size-specific $\delta^{13}C$ and $\delta^{18}O$ in recent planktonic foraminifera. *Paleoceanography* 30:151–73. DOI: 10.1002/2014PA002735.

Fleisher MQ, Anderson RF. 2003. Assessing the collection efficiency of Ross Sea sediment traps using ^{230}Th and ^{231}Pa. *Deep Sea Research, Part II, Topical Studies in Oceanography* 50:693–712.

Francois R, Frank M, Rutgers van der Loeff M, Bacon MP. 2004. ^{230}Th normalization: an essential tool for interpreting sedimentary fluxes during the late Quaternary. *Paleoceanography* 19(1):PA1018. DOI: 10.1029/2003PA000939.

Goreau TJ. 1980. Frequency sensitivity of the deep-sea climatic record. *Nature* 287:620–2 DOI: 10.1038/287620a0.

Guinasso NL, Schink DR. 1975. Quantitative estimates of biological mixing rates in abyssal sediments. *Journal of Geophysical Research* 80:3032–43.

Henderson GM, Anderson RF. 2003. The U-series toolbox for paleoceanography. *Reviews in Mineral Geochemistry* 52:493–531.

Higgins SM, Anderson RF, Marcantonio F, Schlosser P, Stute M. 2002. Sediment focusing creates 100-ka cycles in interplanetary dust accumulation on the Ontong Java Plateau. *Earth and Planetary Science Letters* 203:383–97. DOI: 10.1016/S0012-821X(02)00864-6.

Jaccard SL, Galbraith ED. 2012. Large climate-driven changes of oceanic oxygen concentrations during the last deglaciation. *Nature Geoscience* 5(2):151–6. DOI: 10.1038/ngeo1352.

Jaccard SL, Galbraith ED, Frolicher TL, Gruber N. 2014. Ocean (de)oxygenation across the last deglaciation: insights for the future. *Oceanography* 24(3):162–73. DOI: 10.5670/oceanog.2011.65.

Karlin R, Lyle MW, Zahn R. 1992. Carbonate variations in the northeast Pacific during the late Quaternary. *Paleoceanography* 7(1):43–61.

Keigwin LD. 1998. Glacial-age hydrography of the far northwest Pacific Ocean. *Paleoceanography* 13(4):323–39.

Keigwin LD, Schlegel MA. 2002. Ocean ventilation and sedimentation since the glacial maximum at 3 km in the western North Atlantic. *Geochemistry, Geophysics, Geosystems* 3(6) 10.1029/2001GC000283. DOI: 10.1029/2001GC000283.

Keir RS. 1984. Recent increase in Pacific $CaCO_3$ dissolution: a mechanism for generating old ^{14}C ages. *Marine Geology* 59(1–4):227–50. DOI: 10.1016/0025-3227(84)90095-1.

Keir RS, Michel RL. 1993. Interface dissolution control of the ^{14}C profile in marine sediment. *Geochimica et Cosmochimica Acta* 57(15):3563–73. DOI: 10.1016/0016-7037(93)90139-N.

Kienast SS, Kienast M, Mix AC, Calvert SE, François R. 2007. Thorium-230 normalized particle flux and sediment focusing in the Panama Basin region during the last 30,000 years. *Paleoceanography* 22(2). DOI: 10.1029/2006PA001357.

Kohfeld KE, Chase Z. 2011. Controls on deglacial changes in biogenic fluxes in the North Pacific Ocean. *Quaternary Science Reviews* 30(23–24): 3350–63. DOI: 10.1016/j.quascirev.2011.08.007.

Kozdon R, Ushikubo T, Kita NT, Spicuzza M, Valley JW. 2009. Intratest oxygen isotope variability in the planktonic foraminifer N. pachyderma: real vs. apparent vital effects by ion microprobe. *Chemical Geology* 258(3–4):327–37. DOI: 10.1016/j.chemgeo.2008.10.032.

Laepple T, Huybers P. 2014. Ocean surface temperature variability: large model-data differences at decadal and longer periods. *Proceedings of the National Academy of Science U.S.A* 111 (47):16682–7. DOI: 10.1073/pnas.1412077111.

Lam PJ, Robinson LF, Blusztajn J, Li C, Cook MS, M cmanus JF, Keigwin LD. 2013. Transient stratification as the cause of the North Pacific productivity spike during deglaciation. *Nature Geoscience* 6(8):622–6. DOI: 10.1038/ngeo1873.

Leuschner DC, Sirocko F, Grootes PM, Erlenkeuser H. 2002. Possible influence of Zoophycos bioturbation on radiocarbon dating and environmental interpretation. *Marine Micropaleontology* 46:111–26.

Lisiecki LE, Stern JV. 2016. Regional and global benthic $d^{18}O$ stacks for the last glacial cycle. *Paleoceanography* 31. DOI: 10.1002/2016PA003002.

Lohmann G. 1995. A model for variation in the chemistry of planktonic foraminifera due to secondary calcification. *Paleoceanography* 10(3):445–57.

Löwemark L, Grootes PM. 2004. Large age differences between planktic foraminifers caused by abundance variations and Zoophycos bioturbation. *Paleoceanography* 19(2):1–9. DOI: 10.1029/2003PA000949.

Löwemark L, Werner F. 2001. Dating errors in high-resolution stratigraphy: a detailed X-ray radiograph and AMS-^{14}C study of Zoophycos burrows. *Marine Geology* 177(3–4):191–8. DOI: 10.1016/S0025-3227(01)00167-0.

Lund DC, Mix AC, Southon J. 2011. Increased ventilation age of the deep northeast Pacific Ocean during the last deglaciation. *Nat. Geosci.* 4(11):771–4. DOI: 10.1038/ngeo1272.

Manighetti B, McCave IN, Maslin M, Shackleton NJ. 1995. Chronology for climate change: developing age models for the Biogeochemical Ocean Flux Study cores. *Paleoceanography* 10(3):513–25.

Marcantonio F, Anderson RF, Higgins SM, Stute M, Schlosser P, Kubik PW. 2001. Sediment focusing in the central equatorial Pacific Ocean. *Paleoceanography* 16(3):260–7.

Marchitto TM, Curry WB, Lynch-stieglitz J, Bryan SP, Cobb KM, Lund DC. 2014. Improved oxygen isotope temperature calibrations for cosmopolitan benthic foraminifera. *Geochimica et Cosmochimica Acta* 130:1–11. DOI: 10.1016/j.gca.2013.12.034.

McDonald D. 1993. The late Quaternary history of primary productivity in the Subarctic East Pacific. University of British Columbia.

McManus JF, Anderson RF, Broecker WS, Fleisher MQ, Higgins SM. 1998. Radiometrically determined sedimentary fluxes in the sub-polar North Atlantic during the last 140,000 years. *Earth and Planetary Science Letters* 155:29–43.

McManus JF, Oppo DW, Cullen JL. 1999. A 0.5-million-year record of millennial-scale climate variability in the North Atlantic. *Science* 283(5404):971–5.

Mekik F. 2014. Radiocarbon dating of planktonic foraminifer shells: a cautionary tale. *Paleoceanography* 29(1):13–29. DOI: 10.1002/2013PA002532.

Mekik FA, Anderson RF, Loubere P, François R, Richaud M. 2012. The mystery of the missing deglacial carbonate preservation maximum. *Quaternary Science Reviews* 39:60–72. DOI: 10.1016/j.quascirev.2012.01.024.

Mitchell NC, Huthnance JM. 2013. Geomorphological and geochemical evidence (^{230}Th anomalies) for cross-equatorial currents in the central Pacific. *Deep Sea Research Part I Oceanography Research Papers* 78:24–41 DOI: 10.1016/j.dsr.2013.04.003.

Mollenhauer G, Eglinton TI, Ohkouchi N, Schneider RR, Muller PJ, Grootes PM, Rullkötter J. 2003. Asynchronous alkenone and foraminifera records from the Benguela upwelling system. *Geochimica et Cosmochimica Acta* 67(12):2157–71. DOI: 10.1016/S0016-7037(00)00168-6.

Mollenhauer G, Kienast M, Lamy F, Meggers H, Schneider RR, Hayes JM, Eglinton TI. 2005. An evaluation of ^{14}C age relationships between co-occurring foraminifera, alkenones, and total organic carbon in continental margin sediments. *Paleoceanography* 20(1):1–12. DOI: 10.1029/2004PA001103.

Mollenhauer G, McManus JF, Benthien A, Müller PJ, Eglinton TI. 2006. Rapid lateral particle transport in the Argentine Basin: molecular ^{14}C and $^{230}Thxs$ evidence. *Deep Sea Research. Part I. Oceanography* 53(7):1224–43. DOI: 10.1016/j.dsr.2006.05.005.

Mollenhauer G, McManus JF, Wagner T, McCave IN, Eglinton TI. 2011. Radiocarbon and ^{230}Th data reveal rapid redistribution and temporal changes in sediment focussing at a North Atlantic drift. *Earth and Planetary Science Letters* 301(1–2):373–81. DOI: 10.1016/j.epsl.2010.11.022.

Nozaki Y, Horibe Y, Tsubota H. 1981. The water column distributions of thorium isotopes in the western North Pacific. *Earth and Planetary Science Letters* 54(2):203–16. DOI: 10.1016/0012-821X(81)90004-2.

Ohkouchi N, Eglinton TI, Keigwin LD, Hayes JM. 2002. Spatial and temporal offsets between proxy records in a sediment drift. *Science* 298(5596):1224–7.

Okazaki Y, Timmermann A, Menviel L, Harada N, Abe-Ouchi A, Chikamoto MO, Mouchet A, Asahi H. 2010. Deepwater formation in the North Pacific during the Last Glacial Termination. *Science* 329(5988):200–4.

Oppo DW, McManus JF, Cullen JL. 1998. Abrupt climate events 500,000 to 340,000 years ago: evidence from subpolar North Atlantic sediments. *Science* 279 (5355):1335–8. DOI: 10.1126/science.279.5355.1335.

Peng TH, Broecker WS. 1984. The impacts of bioturbation on the age difference between benthic and planktonic foraminifera in deep sea sediments. *Nuclear Instruments and Methods in Physics Research B* 5(2):346–52. DOI: 10.1016/0168-583X(84)90540-8.

Peng TH, Broecker WS, Berger WH. 1979. Rates of benthic mixing in deep-sea sediment as determined by radioactive tracers. *Quaternary Research* 11(1): 141–9 DOI: 10.1016/0033-5894(79)90074-7.

Pflaumann U. et al. 2003. Glacial North Atlantic: sea-surface conditions reconstructed by GLAMAP 2000. *Paleoceanography* 18(3):1065. DOI: 10.1029/2002PA000774.

Praetorius SK, Mix AC, Walczak MH, Wolhowe MD, Addison JA, Prahl FG. 2015. North Pacific deglacial hypoxic events linked to abrupt ocean warming. *Nature* 527(7578):362–6. DOI: 10.1038/nature15753.

Rae JWB, Sarnthein M, Foster GL, Ridgewell A, Grootes PM, Elliott T. 2014. Deep water formation in the North Pacific and deglacial CO_2 rise. *Paleoceanography* 29:1–23. DOI: 10.1002/2013PA002570.

Reimer PJ. et al. 2013. Intcal13 and Marine13 radiocarbon age calibration curves 0–50,000 years cal BP. *Radiocarbon* 55(4):1869–87.

Ruddiman WF, Glover L. 1972. Vertical mixing of ice rafted volcanic ash in North Atlantic sediments. *Geological Society of America Bulletin* 83(9):2817–36.

Ruddiman WF, McIntyre A. 1981. The North Atlantic Ocean during the last deglaciation. *Palaeogeography, Palaeoclimatology, Palaeoecology* 35:145–214.

Ruddiman WF, Molfino BE, Esmay A, Pokras E. 1980. Evidence beating on the mechanism of rapid deglaciation. *Climate Change* 3:65–87.

Shackleton NJ. 1973. Attainment of isotopic equilibrium between ocean water and the benthonic foraminifera genus Uvigerina: isotopic changes in the ocean during the last glacial. *Proceedings Colloques Internationaux*. Centre National de La Recherche Scientifique. p 203–9.

Skinner LC, Shackleton NJ. 2004. Rapid transient changes in northeast Atlantic deep water ventilation age across Termination I. *Paleoceanography* 19(2):1–12. DOI: 10.1029/2003PA000983.

Spero HJ. 1998. Life history and stable isotope geochemistry of planktonic foraminifera. In Norris R, Corfield RM, editors. *Isotope Paleobiology and Paleoecology*. Volume 4. Paleontological Society Papers. p 7–36.

Stuiver M, Reimer PJ. 1993. Extended ^{14}C database and revised Calib 3.0 ^{14}C age calibration program. *Radiocarbon* 35(1):215–30.

Suman DO, Bacon MP. 1989. Variations in Holocene sedimentation in the North American Basin determined from ^{230}Th measurements. *Deep Sea Research* 36(6):869–78.

Tetard M, Licari L, Beaufort L. 2017. Oxygen history off Baja California over the last 80 kyr: a new foraminiferal-based record. *Paleoceanography*. 246–64. DOI: 10.1002/2016PA003034.

Trauth MH. 2013. TURBO2: A MATLAB simulation to study the effects of bioturbation on paleoceanographic time series. *Computers & Geosciences* 61:1–10. DOI: 10.1016/j.cageo.2013.05.003.

Uchida M, Shibata Y, Ohkushi K, Yoneda M, Kawamura K, Morita M. 2005. Age discrepancy between molecular biomarkers and calcareous foraminifera isolated from the same horizons of Northwest Pacific sediments. *Chemical Geology* 218(1–2):73–89. DOI: 10.1016/j.chemgeo.2005.01.026.

Waelbroeck C, Duplessy JC, Michel E, Labeyrie L, Paillard D, Duprat J. 2001. The timing of the last deglaciation in North Atlantic climate records. *Nature* 412(6848):724–7. DOI: 10.1038/35106623.

Wheatcroft RA, Jumars PA, Smith CR, Nowell ARM. 1990. A mechanistic view of the particulate biodiffusion coefficient: step lengths, rest periods and transport directions. *Journal of Marine Research* 48(1):177–207. DOI: 10.1357/002224090784984560.

Wycech J, Clay Kelly D, Marcott S. 2016. Effects of seafloor diagenesis on planktic foraminiferal radiocarbon ages. *Geology* 44(7):551–4. DOI: 10.1130/G37864.1.

Yarincik KM, Murray RW, Lyons TW, Peterson LC, Haug GH. 2000. Oxygenation history of bottom waters in the Cariaco Basin, Venezuela, over the past 578,000 years: results from redox-sensitive metals (Mo, V, Mn, and Fe). *Paleoceanography* 15(6):593–604.

Žarić S, Donner B, Fischer G, Mulitza S, Wefer G. 2005. Sensitivity of planktic foraminifera to sea surface temperature and export production as derived from sediment trap data. *Marine Micropaleontology* 55(1–2):75–105. DOI: 10.1016/j.marmicro.2005.01.002.

Zheng Y, Van Geen A, Anderson RF, Gardner JV, Dean WE. 2000. Intensification of the northeast Pacific oxygen minimum zone during the Bolling-Allerod warm period. *Paleoceanography* 15(5):528–36.